Influence of Water Balance and Classifier Choice on Energy Efficiency of Milling Circuits

Adrian Hinde[1*], Elizma Ford[2], Jean Makola[3] and Amit Jain[4]

[1]Independent Comminution Consultant, Johannesburg, South Africa
[2]Mintek, Randburg, South Africa
[3]Derrick Solutions International, Johannesburg, South Africa
[4]Derrick Corporation, Buffalo, New York, USA

**Corresponding author: adrianh@icon.co.za*

A large contributor to the energy consumption of metallurgical plants is the mill circuit. A popular circuit configuration is one involving a primary open-circuit semi-autogenous mill followed by a secondary ball mill operating in a closed circuit with hydrocyclones. The objective of the secondary circuit is not only to minimise the energy required to liberate the valuable mineral species but also to yield a product that optimises the residence time of the downstream leach tanks and/or flotation cells. Unfortunately, the energy-efficient operation of the milling circuit implies that the hydrocyclones must be fed at low pulp densities (corresponding to about 20% solids by volume). This results in a very dilute circuit product, leading to sub-optimal residence times for the leaching tanks or flotation cells, which should also be fed at pulp densities of about 20% by volume. Accordingly, the hydrocyclone overflow product should be dewatered and thickened before it can be treated downstream. It is shown how high classification and overall plant efficiencies can be achieved by using in-circuit dewatering hydrocyclones and by replacing the classifying hydrocyclones with modern fine screening technology.

INTRODUCTION

It is generally acknowledged that energy up to 50% of that utilised by base metal and gold mines worldwide can be attributable solely to comminution (Ballantyne and Powell 2014; Bleiwas, 2011). Accordingly, there is considerable incentive to find ways of minimising the energy consumed by milling circuits, comprising mills closed by hydrocyclone classifiers, which can have a significant influence on the overall energy efficiency of the circuit. Figure 1 shows a basic circuit configuration involving a primary semi-autogenous (SAG) mill followed by a closed circuit ball mill.

The classification efficiency of a hydrocyclone is determined by its partition function, giving recoveries of solids in individual size classes and water to the underflow stream. One source of inefficiency relates to the fraction of the feed solids reporting directly to the underflow without classification. This bypass fraction increases with increasing solids concentration of the feed pulp. One approach for sourcing water to control the pulp density to the classifying hydrocyclones is shown in Figure 2. However, optimising the energy efficiency of the milling circuit implies very dilute overflow pulp densities, leading to sub-optimal residence times for the downstream flotation cells and leaching tanks. It will be shown how this conundrum can be resolved by making use of in-circuit dewatering hydrocyclones and replacing the classifying hydrocyclones with modern fine screening technology.

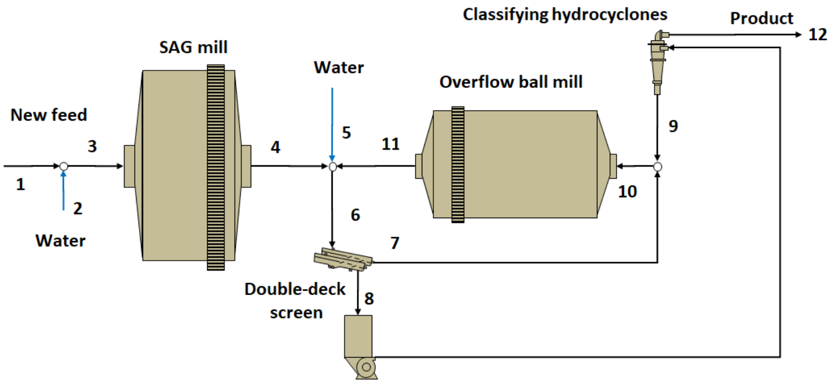

Figure 1: Basic two-stage milling circuit.

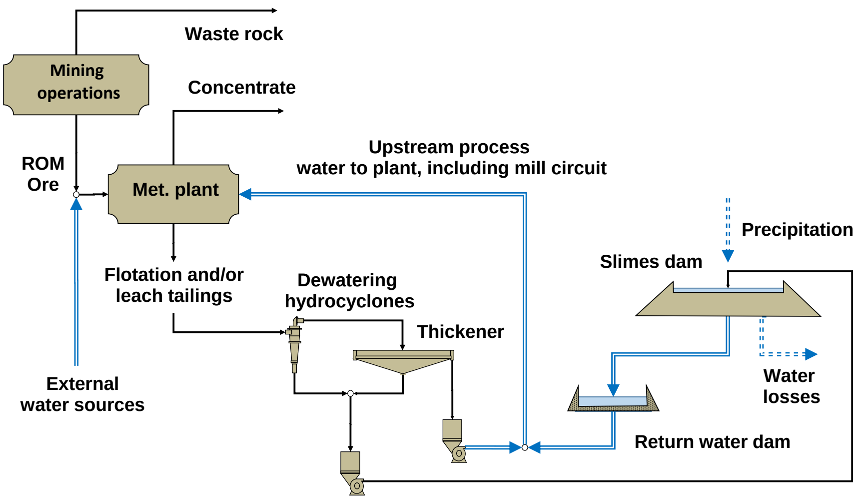

Figure 2: A Conventional approach to recycling water for milling circuits.

MODELLING

To understand the behaviour of milling circuits, it is helpful to make use of simple phenomenological models to quantify the breakage kinetics and material transport behaviour of ore in both the autogenous (AG)/SAG mill and ball mill. It is also helpful to model the performance of the hydrocyclones and screens in terms of a partition function, giving the recoveries of particles of a given size to the oversize stream, along with the recovery of water.

For primary AG/SAG mills, with high aspect ratios (ratio of internal mill diameter to effective grind length), it is usually assumed that the mill can be treated as a single fully mixed reactor with grinding kinetics that can be modelled by invoking the concept of an energy-based cumulative breakage rate function. Material transport behaviour in primary AG/SAG mills can be modelled in terms of a specific discharge rate function, which is defined as the ratio of the discharge mass flow rate of particles in a given size class to the mass hold-up of particles in the same size class. Although it is impractical to measure hold-up ore masses and particle size distribution at production scale, useful information can be obtained from pilot tests using mill with diameters in the range 1.5 m to 1.8 m and effective grind lengths in the range 0.4 to 0.6 m (Hinde and Kalala, 2008a). The specific discharge rate function is determined by the geometry of the discharge grate, such as the aperture sizes and open areas. It is important to appreciate that size classification is best modelled as a weighted sum of classification through the grate apertures and through the voids between rocks too large to pass through the grate apertures.

The grinding kinetics of overflow ball mills can be modelled in a similar way to AG/SAG mills using a simplified version of the cumulative breakage rate function. Material transport behaviour can be modelled by treating the mill as three fully mixed reactors in series with no classification at the overflow lip. The detailed formulation of the mathematical structure of the cumulative breakage function has previously been described in detail by Hinde and Kalala (2008b). However, there have been some updates to the model structure for the energy-based cumulative specific breakage rate function, which are discussed below.

Cumulative Breakage Rate Function

An energy-based five-parameter equation for the cumulative specific breakage rate function, applicable to both SAG and ball mills, is given by:

$$\mathrm{K}_i^E = \kappa_1 \left\{ \frac{1-\exp\left(-\left(\frac{x_i}{a}\right)^{\alpha_1}\right)}{1-\exp\left(-\left(\frac{1}{a}\right)^{\alpha_1}\right)} + \kappa_2 {x_i}^{\alpha_2} \right\}; \;\; a \neq 0 \qquad [1]$$

In Equation 1, x_i refers to the upper size limit of particles in size class i, $(i = 1,2,3,\cdots n)$. By convention, the mesh sizes conform to a root-two geometric progression of standard sieve sizes. The sink size class, $i = n$, refers to all particles with mesh sizes less than x_n, with a lower limit of zero. The model parameters in Equation 1 are given by κ_1, κ_2, α_1, α_2 and a. For AG/SAG mills, the parameters can be back-calculated from tests conducted using a pilot-scale mill with feeds that cover a comple spectrum of particle and rock sizes likely to be encountered at production scale (80% passing size of about 150 mm and a top size around 250 mm). For ball milling applications, where the top size is usually less than 16 mm, the parameters can be estimated from batch tests using a laboratory-scale mill (Herbst and Fuerstenau, 1971). It should be noted that Equation 1 is a monotonically increasing function of particle size. It is pertinent to point out that other researchers (Amestica *et al.*, 1993)) use the following non-monotonic form:

$$\mathrm{K}_i^E = \kappa_1 \frac{\hat{x}_i^{\alpha_1}}{1+\left(\frac{\hat{x}_i}{\mu}\right)^{\lambda}} + \kappa_2 x_i^{\alpha_2} \qquad [2]$$

Unfortunately, it was found that parameters obtained from open-circuit pilot tests using Equation 2 can lead to simulation predictions for closed-circuit operation with small negative flows in some of the size classes.

For milling applications involving overflow ball mills, it was found that the parameter κ_2 in Equation 1 could be assumed to be zero, leading to a simple three-parameter model. These parameters can be back-calculated from laboratory batch milling tests using an instrumented mill that allows for the monitoring and recording of the mechanical power transmitted to the mill charge.

Figure 3 gives an example of the measured size distributions and model fits for net specific energy inputs of 10 kW/t, 20 kWh/t and 40 kW/t. For batch milling tests, the residence time distribution is identical to a plug-flow residence time distribution for a continuously fed mill. The relationship between the product size distribution, the feed size distribution and the specific energy input is given by:

$$P_i(\xi) = (1 - F_i)\exp(-\xi \mathrm{K}_i^E) \qquad [3]$$

In Equation 3, $P_i(\xi)$ is the mass fraction smaller than x_i in the mill, expressed as a function of specific energy, ξ. The mass fraction less than x_i in the feed is given by F_i.

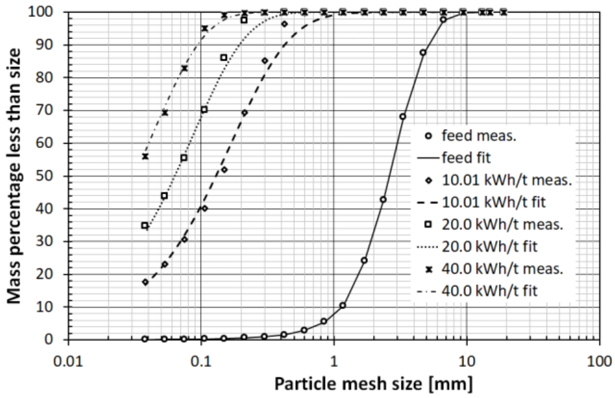

Figure 3: Model fits to batch data.

Once the specific cumulative breakage rate function has been derived from batch ball milling tests, it is possible to predict the performance of a continuously fed production mill, which can be modelled as three fully mixed reactors in series. The cumulative product size distribution, P_i, (the mass fraction less than given size) for each reactor can be related to the inlet cumulative size distribution by the following equation:

$$P_i = \frac{F_i + \xi \mathrm{K}_i^E}{1 + \xi \mathrm{K}_i^E} \quad [4]$$

where ξ [kWh/t] is the specific energy defined as the net mill power divided by inlet mass flow. Conversely, it is possible to calculate the individual values of the cumulative breakage rate for each size class from the following equation:

$$K_i^E = \frac{1}{\xi}\left(\frac{P_i - F_i}{1 - P_i}\right) \quad [5]$$

A similar approach can be adopted for a SAG mill, leading to the following estimates of the cumulative breakage rate function for each size class, which can be estimated from pilot data (assuming $x_{max} < x_1$).

In the following equations, f_i and p_i are the feed and discharge flows in each size class, respectively. The net mill power and the total holdup mass of ore in the mill are given by P_{mill} [kW] and M[t], respectively.

For i = 1:

$$\mathrm{K}_2^E = \frac{f_1 - p_1}{w_1 P/M} \quad [6]$$

For $i = 2, 3, \cdots, n$:

$$\mathrm{K}_{i+1}^E = \frac{f_i - p_i + W_i (P/M)\mathrm{K}_i^E}{(w_i + W_i)P/M} \quad [7]$$

For $i = n$:

$$\mathrm{K}_n^E = \frac{p_n - f_n}{W_n P_{mill}/M} \quad [8]$$

The above equations were applied to data generated from open-circuit pilot tests using an Aerofall mill treating a Cu, Au, Mo ore from Argentina. The mill had an internal diameter of 1.67 m and effective grind length of 0.56 m. The mill was operated at an angular velocity 75% of critical. The mill tests were run using two peripheral discharge grates, each with three slots. The slots were about 155 mm in length and about 9 mm wide. Open-circuit tests were run with the mill running fully autogenously and at ball loads of 3%, 6%, 9% and 12 %. Figure 4 shows the raw data as markers and the model fits as lines. Feed rates were adjusted (using a proportional-integral feedback loop) to control the charge volume close to 30% of the mill volume in all cases. It is pertinent to point out that similar trends were reported by Austin *et al*. (1993).

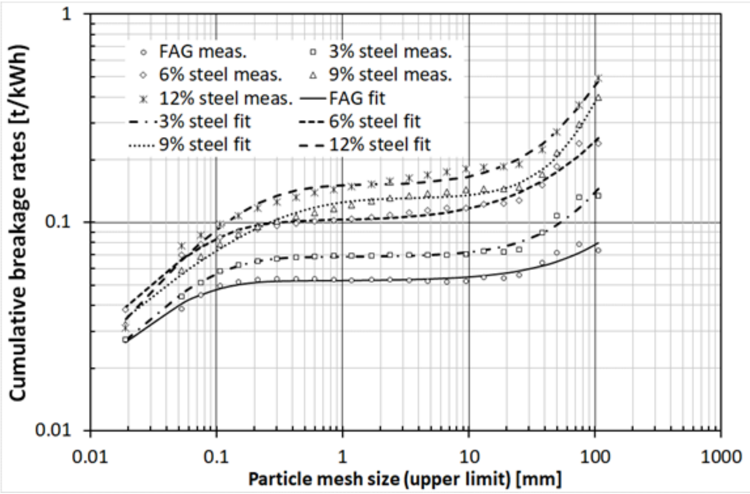

Figure 4: Cumulative specific breakages for an Argentinian Cu ore.

Specific discharge rate function for SAG mills

The specific discharge rate function (g_i) is defined as the ratio of the discharge flow of solids in a given size class to the corresponding holdup mass. This function is usually expressed as the product of the specific water recovery and a classification function, ($g_i = g_w c_i$) and is often assumed to be a simple monotonically decreasing function of particle size (Napier-Munn *et al*., 1996). However, there is evidence (Amestica *et al*., 1993) that the classification function can be non-monotonic. One explanation of this apparently anomalous behaviour is that the effective aperture size of particles in fine and intermediate size ranges are controlled by the effective void size of particles in the coarse size range (coarser than the aperture size of the grate), rather than the grating aperture size. It was assumed that the overall classification function has the form:

$$c_i = 1 - \left[\beta_i c_i^{fines} + (1 - \beta_i) c_i^{coarse}\right] \quad [9]$$

where the weighting function, β_i is given by a logistics function:

$$\beta_i = \frac{1}{1 + \left(\frac{\hat{x}_i}{d_{50}}\right)^{\alpha_1}} \quad [10]$$

The classification function for the fines is given by:

$$c_i^{fines} = 1 - \exp\left[\ln(0.5)\left(\frac{x_i}{d_{50}^{fines}}\right)^{\alpha_2}\right] \quad [11]$$

The classification for coarse particles is given by a truncated Rosin–Rammler distribution:

$$c_i^{coarse} = \frac{1 - \exp\left[-a\left(\frac{\hat{x}_i}{d_{max}}\right)^{\alpha_3}\right]}{1 - \exp(-a)} \qquad a \neq 0\,, \quad x_i \leq d_{max} \qquad [12]$$

$$c_i^{coarse} = 1 \qquad x_i > d_{max} \qquad [13]$$

The above model for the specific discharge rate function was applied to the same data obtained from the pilot tests used to determine the cumulative breakage rate function described above. Figure 5 shows the measured specific discharge rates as markers and the model fits as continuous lines. It is clear that the measured data are subject to considerable scatter. This is perhaps not surprising since the charge mass fractions in the mid-size range had values close to zero. In other words, the holdup size distribution showed a tendency to be gap-graded. This implied that errors of less than 1% in the mass fraction could lead to major variations in the measured specific discharge rates. Similar high levels of scatter were recently reported in an MSc. thesis derived from grind-out tests conducted in a 1.8 m diameter mill batch mill (Mitchell, 2015). Nonetheless, the model fits obtained in Mitchell's study and the results shown in Figure 5 show clear evidence of inflexion points in the plotted specific discharge functions.

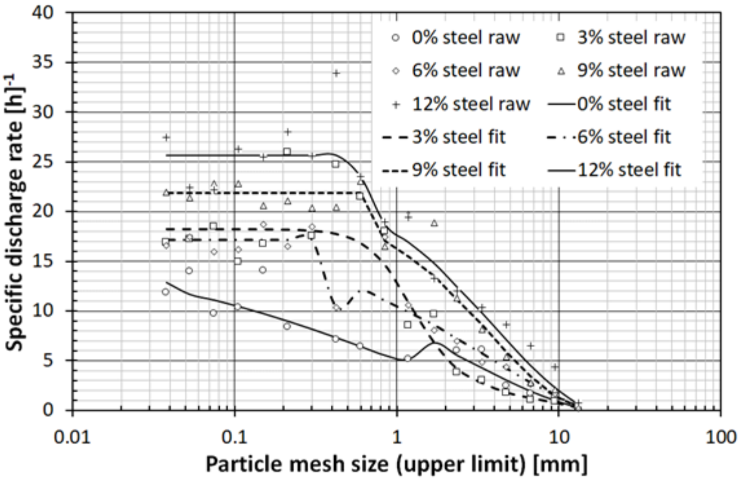

Figure 5: Specific discharge rates derived from pilot tests.

Modelling Partition Function for Hydrocyclones and Vibrating Screens

The partition functions for both hydrocyclones and screens can be modelled as a weighted sum of two separate functions, one of which accounts for the primary classification effect and the other is a secondary short-circuiting effect due to water entrainment. For hydrocyclones, the partition function for primary classification can be modelled in terms of a number two-parameter probabilistic functions, including the ubiquitous Rosin–Rammler function, which takes the form:

$$R_i = 1 - \exp\left(\ln(0.5)\left(\frac{\hat{x}_i}{d_{50c}}\right)^m\right) \approx 1 - exp\left(-0.6931\left(\frac{\hat{x}_i}{d_{50c}}\right)^m\right) \qquad [14]$$

In Equation 14, the geometric mean size for particles in size class i is given by $\hat{x}_i$ (by convention, an arithmetic mean is used for the sink class, i.e., $\hat{x}_n = x_n/2$. Unfortunately, this function does not have a finite upper size limit above which particles cannot report to the undersize stream. In other words, this function asymptotes to a value of unity only at infinite particle size.

The primary partition function for screens over a standard sieve size range down to 38 µm can usually be quantified in terms of a truncated Rosin–Rammler distribution having a finite truncation size d_{mesh} corresponding to the *effective* mesh size of the screen. The effective mesh size can be defined as the finite upper limit above which particles above this this size cannot pass through the screen.

Obviously, any particles with mesh sizes coarser than d_{mesh} will always report to the oversize stream. This truncated partition function takes the following form:

$$R_i = r_f + (1 - r_f) \cdot \frac{1 - \exp\left[-a\left(\frac{\hat{x}_i}{d_{mesh}}\right)^m\right]}{1 - \exp(-a)} \qquad a \neq 0 \qquad \hat{x}_i \leq d_{mesh} \tag{15}$$

$$R_i = 1 \qquad \hat{x}_i > d_{mesh}$$

In Equation 15, $\hat{x}_i$ is the geometric mean size of particles in size class i with upper and lower limits of x_i and x_{i+1}, respectively. These sizes are assumed to follow a root-two geometric progression $(x_1, x_2, \cdots, x_n)$ with the sink size class covering a size range from zero to x_n.The function r_f allows for the effects of classification due to water entrainment at fines sizes and can be related to the water split, r_w, (fractional recovery of water to oversize) by an equation of the following form:

$$r_f(\hat{x}_i) = \frac{r_w}{1 + \left(\frac{\hat{x}_i}{\delta}\right)^\gamma} \tag{16}$$

The parameter a can take on both negative and positive values, which influences the slope of the partition plot at coarse sizes. In the limit as ($a \to 0$), the distribution takes the form of the familiar Gaudin–Schuhmann distribution, which plots as a straight line on a log–log scale.

The difference between the partition functions for a screen and hydrocyclone (treating the same material) is that is that the parameter m (the slope of the partition plot) is much larger for the screen, as shown in Figure 6. The reason for this can easily be explained by the fact that most ores are comprised of a mixture of different mineral species with different specific gravities. In other words, the overall partition function is a weighted sum of a number of different partition functions, unlike a screen where the partition function is insensitive to differences in particle specific gravities.

It should be appreciated that the effective mesh size of urethane screens is significantly greater than the stated nominal static mesh size This is due to the mesh flexing during vibration to prevent blinding. Moreover, the apertures have a rectangle shape with the length several times longer than the width. The latter dimension is referred to as the nominal stated size. Another useful property of urethane is that it has a much higher hydrophilicity index than stainless steel. This fact implies that urethane panels can significantly reduce the amount of water and entrained undersize material reporting to the oversize stream. Urethane screen mesh also has a much longer operating life than steel mesh.

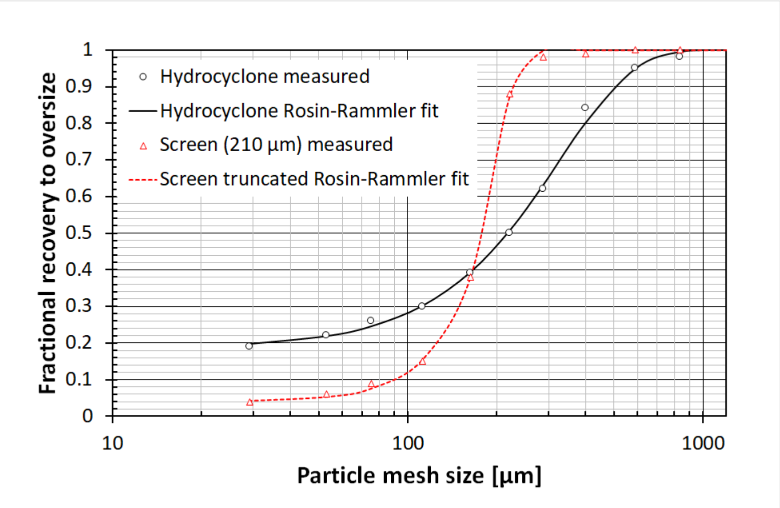

Figure 6: Partition functions for hydrocyclone and screen.

Size distributions are usually determined routinely by wet and dry sieving techniques down to about 38 µm. At sizes below 38 µm, laser diffraction sizing techniques provide an attractive alternative to sieving. These sizing techniques can cover a spectrum of sizes spanning a range from about 100 nm up to about 2 mm.

The parameters δ and γ can be determined using back-calculation methods by minimising a weighted sum of squares of the relative differences between the measured partition function coefficients and the model fits given by Equations 15 and 16. Figure 7 shows measurements of the feed size distribution and partition plot for a 100 µm mesh screen obtained by Derrick at their test facility in the USA. The test facility is fitted with a single deck. To predict the performance of a five-deck production scale Stacksizer, one must multiply the measured test throughput by a factor of five. The reported production scale results were predictions based on a solids feed rate of 57 t/h. The total feed rate for the water (including spray water) was 114 m^3/h. These feed rates are consistent with a feed pulp density corresponding to about 30% solids by mass or 10% solids by volume. This feed density is significantly lower than the maximum recommended by Derrick (15% solids by volume). Tests were conducted on a chrome-rich ore having a specific gravity of 3.80. It should be noted that although the mesh had a nominal mesh size of 100 µm, particles significantly greater than 150 µm could pass through the screen for the reasons explained earlier.

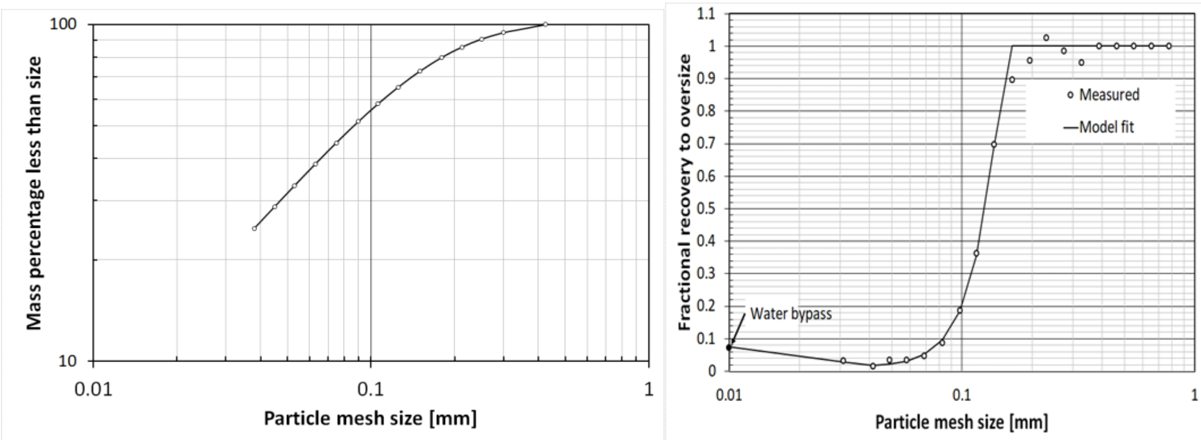

Figure 7: Feed size distribution and partition plot from Stacksizer tests.

Figure 8 shows partition plots determined using Derrick's test facility at Mintek in South Africa (Mwale and Mainza, 2016), but using laser diffraction techniques to measure size distributions. These plots show the raw test data and model fits based on Equations 15 and 16. These techniques, coupled with factorial experimental designs (Ford *et al.*, 2016) offers considerable scope for developing improved phenomenological models for both hydrocyclones and modern fine screening technology.

SIMULATION STUDY

In this study, consideration is given to three scenarios using the pilot data reported earlier and the derived models for hydrocyclones and screens. The first case involves a basic circuit involving the pilot SAG mill operating in open circuit at a static ball charge of 12% of mill volume and a total charge volume occupying about 30% of mill volume. Consideration is then given to a scenario where a cluster of dewatering hydrocyclones is included in the circuit. In the final scenario, the classifying hydrocyclones are replaced with vibrating screens. In each case, the circuit is constrained to achieve a target grind corresponding to 80% passing size of 75 µm and a pulp density corresponding to 45% solids by mass, considered to be optimal for downstream leaching or flotation.

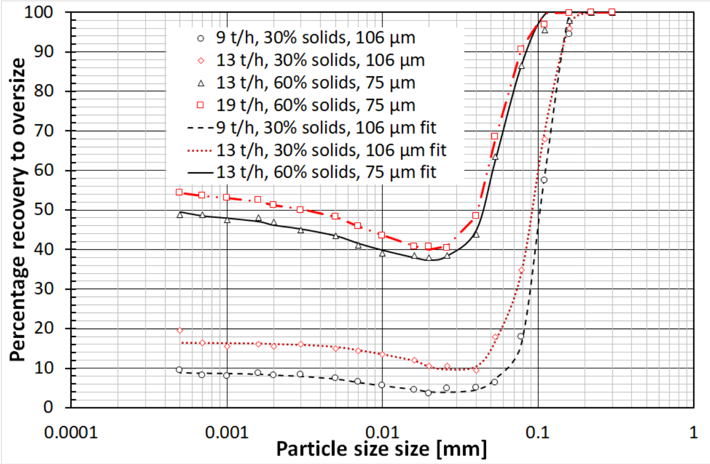

Figure 8: Partition plots at sub-sieve sizes (Mwale et al., 2016).

Scenario 1: Base Case
Figure 1, shown earlier, shows the base case circuit involving the pilot SAG mill operating at a ball charge 12% of the mill volume. The mill discharge is fed to a conventional double-deck screen with a lower deck mesh size of 1 mm. Piloting tests conducted at Mintek have shown that the combined oversize products (with a pulp density corresponding to about 85% solids by mass) can be easily be conveyed to the ball mill inlet using pocketed conveyors.

The cumulative breakage rate function for the ball mill was derived from standard batch milling tests, as described earlier. The residence time distribution was modelled by treating the ball mill as three fully mixed reactors in series (volume ratios of 0.7: 0.15: 0.15).

The results of the simulation study showed that the net power consumed by the ball mill to meet the final target grind and pulp density was 25.4 kW. Given the measured mill power for the SAG mill, based on the pilot data (13.17 kW), the overall energy efficiency for the circuit turned out to be 28.0 kWh per tonne of new −75 µm product.

Scenario 2: In-Circuit Dewatering
In this scenario, a cluster of dewatering hydrocyclones (nominal diameters around 100 mm diameter) were incorporated into the circuit, capable of cut-sizes of around 10 µm. The objective of using dewatering hydrocyclones is to reduce the pulp density to the classifying hydrocyclones, thereby reducing the bypass inefficiency parameter (Englebrecht, 1977). It turns out that the ‘fishhook’ effect becomes clearly evident at sub-sieve sizes (Neese *et al.*, 2015). The flowsheet for this configuration is shown in Figure 9.

The results of the simulation showed that the power requirement for the ball was reduced to 18.1 kW. The overall specific energy efficiency of the milling circuit was reduced to from 28.0 kWh/t−75µm to 21.3 kWh/t−75 µm, without sacrificing the grind size and pulp density of the circuit product.

Scenario 3: Replacing Classifying Hydrocyclones with Stacksizers
The third scenario is similar to the second one, but with the classifying hydrocyclones replaced with Stacksizer screens. The flowsheet for this scenario is shown in Figure 10. In this case, the ball mill power was 14.07 kWh, giving overall specific energy for the circuit of 18.6 kWh/t−75 µm.

The power ball required by the mills to achieve the target grind of 80% passing 75 µm for the three different scenarios are summarised in Table I. In all cases, the power consumed by the SAG mill was 13.2 kW.

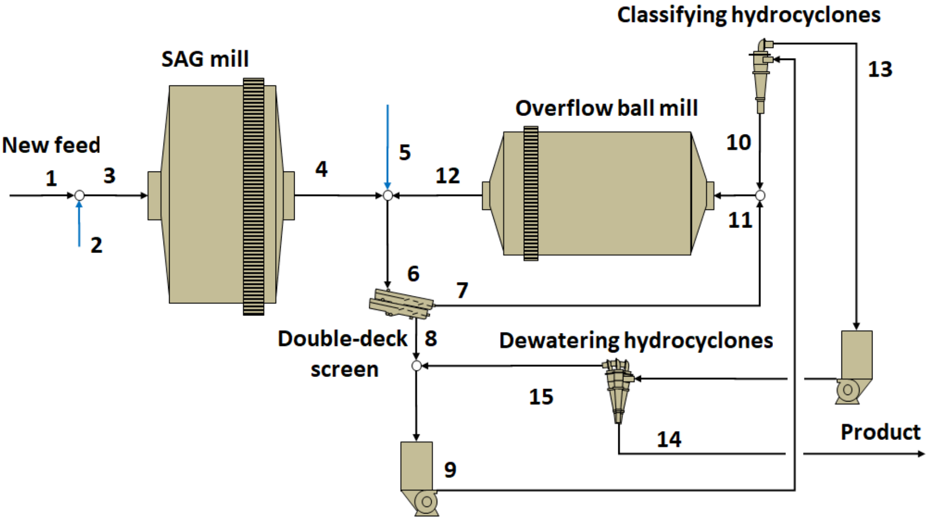

Figure 9: Flowsheet for a scenario using dewatering hydrocyclones.

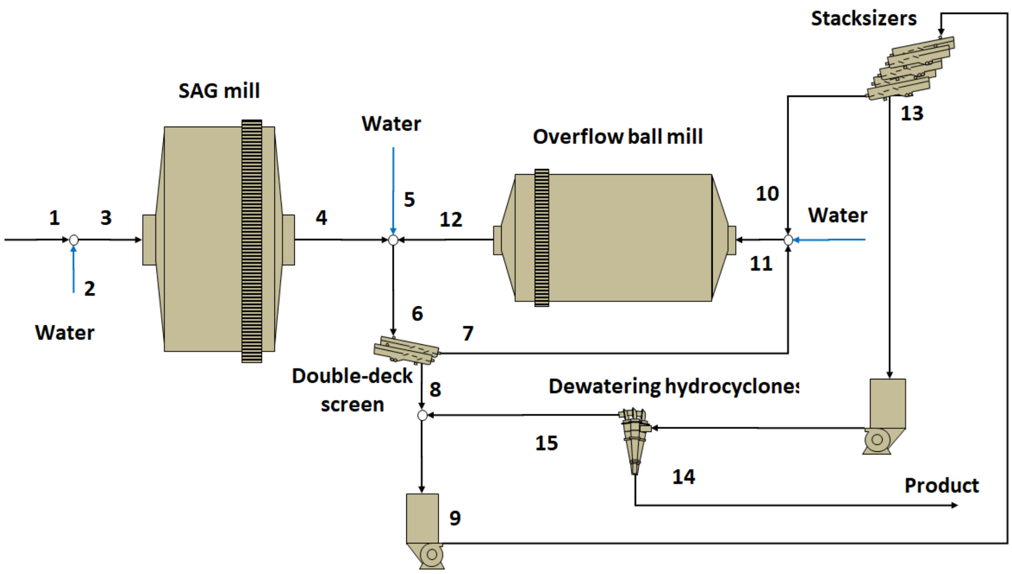

Figure 10: Flowsheet with classifying hydrocyclones replaced with screens.

Table I: Power requirement and energy efficiencies.

Scenario	Ball mill (kW)	Secondary circuit (kWh/t −75 µm)	Overall circuit (kW)	Overall circuit (kWh/t −75 µm)
1	20.45	24.06	33.62	22.91
2	17.65	20.77	30.82	21.00
3	14.07	16.56	27.24	18.56

It can be seen from Table I that the energy efficiency improvements with respect to both in-circuit dewatering and replacing the hydrocyclones with the Stacksizer screens are significant.

It should also be noted that there is scope for improving the efficiency and throughput of the primary circuit by fitting discharge grate with pebble ports and operating the mill in closed circuit with a recycle crusher.

CONCLUSIONS

It has been argued that there is considerable scope for improving the energy efficiency of grinding circuits treating metalliferous ore (up to about 30 percent improvements in energy efficiency without sacrificing the grind size or throughput capacity. This can be achieved through the innovative exploitation of available water resources and replacing conventional classifying hydrocyclones with modern fine screening technology. Although the use of in-circuit dewatering hydrocyclones to improve mill circuit energy efficiencies does not seem to be widely practised, there is at least one mine that has exploited the concept successfully (Ncube, 2015) and has been able to provide pulp densities for leaching as high as 52 percent solids by mass.

Although there are significant benefits to be gained from using screens as classifying devices, it is obviously important to consider the economic trade-offs between the financial benefits and the costs involved with replacing hydrocyclones with screens. Should one follow a strategy of maintaining the same plant throughput but increasing metal recoveries by grinding finer, or should one increase plant throughput, without sacrificing the grind size? One can, of course, follow a strategy of doing both. Derrick Corporation has conducted a number of studies in collaboration with their clients to explore these scenarios for copper ores. From these analyses, it was estimated in most cases the investment costs incurred by the copper mine could be recouped in less than 12 months.

To conclude, it should be noted there are approximately 500 Derrick Stack Sizers operational in the closing of milling circuits in the world. At Derrick, we are not aware of a single failed installation where Stack Sizers replaced hydrocyclones. In total, there are close to 2000 Stack Sizers in operation with 280 Derrick screens in Africa. It is perhaps pertinent to ask why most plants continue to close their milling circuits with hydrocyclones. With high capacity operations, typically copper, the number of screens required can be daunting to operators. They accept large numbers of gravity spirals, flotation cells and other concentration devices, but when it comes to screens, they seem to have a mental block. This seems to be true even though the net present profit obtained over the remaining life of the mine life of the mine can be phenomenal. There is, of course, the capital required, and here we also experience reluctance as these costs could be perceived to be prohibitive. This is particularly true in the early stages of evaluation where pre-feasibility studies multiply major capital equipment costs by a risk factor as high as 4, which overestimates the project when high-value equipment is considered.

ACKNOWLEDGEMENTS

The historical data presented in this report were derived from tests conducted at Mintek, Johannesburg, South Africa, and at Derrick Corporation's test facility, Buffalo, USA.

REFERENCES

Améstica, R., Gonzáles, G.D., Barria, J., Magne, L., Menacho., J.M., Castro, O. (1993). A SAG mill circuit dynamic simulator based on a simplified mechanistic model. *Proceedings, XVIII International Mineral Processing Congress Congress*. Australasian Institute of Mining and Metallurgy, Parkville, Vic,. Australia. pp. 117–129.

Austin, L.G., Menacho, J.M., Pearcy, F. (1987). A general model for semi-autogenous and autogenous grinding. *Proceedings APCOM Proceedings of the Twentieth International Symposium on the Application of Computers and Mathematics in the Mineral Industries. Volume 2: Metallurgy.* Southern African Institute of Mining and Metallurgy, Johannesburg. pp. 107–126.

Austin, L.G., Sutherland., D.N., Gottlieb, P. (1993). An analysis of SAG mill frinding and liberation tests. *Minerals Engineering,* 6 (5), 491–507.

Ballantyne, G.R., Powell, M.S. (2014). Benchmarking comminution energy consumption for the processing of copper and gold ores. *Minerals Engineering,* 65, 109–114.

Bleiwas, D.I. (2011). Estimates of electricity requirements for the recovery of mineral commodities, with examples applied to Sub-Saharan Africa. Open-File Report-1253, U.S. Department of the Interior US Geological Society. https://pubs.usgs.gov/of/2011/1253/report/OF11-1253.pdf [accessed 20 Mar. 2018].

Englebrecht, J.A. (1977). The effect of classification efficiency on milling and its economic significance. *Vacation School: Grinding – Theory and Practice*. South African Institute of Mining and Metallurgy, Johannesburg.

Ford, E., Mudau, P., Hinde. A., Jain, A., Barkhuysen, N. (2016). Evaluating the potential throughput benefit of adopting Derrick fine screening technology in a PGM slag ball mill circuit. Unpublished conference proceedings, *Comminution 2016*, Minerals Engineering International, http://www.min-eng.com/ (reference accessed 20 March 2017).

Herbst, J.A., Fuerstenau, D.W. (1973). Mathematical simulation of dry ball milling using specific power information. *Trans. AIME*, 254, 343–348

Hinde, A.L., Kalala, J.T. (2008a). Pilot and laboratory test procedures for the design of semi-autogenous grinding circuits treating platinum ores. *Third International Platinum Conference. Platinum in Transformation.* Paper 58, pp. 1-12. Southern African Institute of Mining and Metallurgy, Johannesburg, South Africa.

Hinde, A.L., Kalala, J.T. (2008b). The application of a simplified approach to modelling tumbling mills, stirred media mills and HPGRs. *Minerals Engineering*, 22, 633–641.

Latchreddi, S., Morrell, S. (2003). Slurry flow in mills: grate-only discharge mechanism (Part 1). *Minerals Engineering,* 16, 625–633.

Latchreddi, S., Morrell, S. (2003). Slurry flow in mills: grate-only discharge mechanism (Part 2). *Minerals Engineering,* 16, 635–642.

Mitchell, D. (2015). Improved relationships for discharge in SAG/AG. MSc. thesis (SMI), JMRC. https://espace.library.uq.edu.au/view/UQ:370609/s4171764_mphil_submission.pdf (accessed 20 March 2018).

Mokken, A.H., Blendulf, G.K.I. (1975). A study of the arrangements for pulp discharge on pebble mills, and their influence on mill performance. *Journal of the South African Institute of Mining and Metallurgy,* 10, 257–289.

Mwale, A.N., Mainza, A.N., Bepswa, P.A., Simukanga, S., Masinja, J. (2016). Model for fine wet screening. Proceedings *IMPC2016: XXVII International Mineral Processing Congress.* Canadian Institute of Mining, Metallurgy and Petroleum, Montreal. pp. 1–11.

Napier-Munn, T.J., Morrell, S., Morrison, R.D., Kojovic, T. (1996). *Mineral cComminution Circuits: Their Operation and Optimisation*. JKMRC Monograph Series in Mining and Mineral Processing. Vol. 2.

Ncube, T. (2015). Freda Rebecca SAG milling circuit optimisation. https://core.ac.uk/download/pdf/39676178.pdf [accessed 20 Mar. 2018].

Neesse, Th., Dueck, J., Schwemmer, H., Farghaly, M. (2015). Using a high-pressure hydrocyclone for solids classification in the submicron range. *Minerals Engineering,* 71. pp.85–88.